Journal of Medical Imaging

MedicalImaging.SPIEDigitalLibrary.org

Android application for determining surgical variables in brain-tumor resection procedures

Rohan C. Vijayan
Reid C. Thompson
Lola B. Chambless
Peter J. Morone
Le He
Logan W. Clements
Rebekah H. Griesenauer
Hakmook Kang
Michael I. Miga

SPIE.

Rohan C. Vijayan, Reid C. Thompson, Lola B. Chambless, Peter J. Morone, Le He, Logan W. Clements, Rebekah H. Griesenauer, Hakmook Kang, Michael I. Miga, "Android application for determining surgical variables in brain-tumor resection procedures," *J. Med. Imag.* **4**(1), 015003 (2017), doi: 10.1117/1.JMI.4.1.015003.

Android application for determining surgical variables in brain-tumor resection procedures

Rohan C. Vijayan,[a] Reid C. Thompson,[b] Lola B. Chambless,[b] Peter J. Morone,[b] Le He,[b] Logan W. Clements,[a] Rebekah H. Griesenauer,[a] Hakmook Kang,[c] and Michael I. Miga[a,b,d,*]
[a]Vanderbilt University, Department of Biomedical Engineering, Nashville, Tennessee, United States
[b]Vanderbilt University Medical Center, Department of Neurological Surgery, Nashville, Tennessee, United States
[c]Vanderbilt University Medical Center, Department of Biostatistics, Nashville, Tennessee, United States
[d]Vanderbilt University Medical Center, Department of Radiology and Radiological Sciences, Nashville, Tennessee, United States

Abstract. The fidelity of image-guided neurosurgical procedures is often compromised due to the mechanical deformations that occur during surgery. In recent work, a framework was developed to predict the extent of this brain shift in brain-tumor resection procedures. The approach uses preoperatively determined surgical variables to predict brain shift and then subsequently corrects the patient's preoperative image volume to more closely match the intraoperative state of the patient's brain. However, a clinical workflow difficulty with the execution of this framework is the preoperative acquisition of surgical variables. To simplify and expedite this process, an Android, Java-based application was developed for tablets to provide neurosurgeons with the ability to manipulate three-dimensional models of the patient's neuroanatomy and determine an expected head orientation, craniotomy size and location, and trajectory to be taken into the tumor. These variables can then be exported for use as inputs to the biomechanical model associated with the correction framework. A multisurgeon, multicase mock trial was conducted to compare the accuracy of the virtual plan to that of a mock physical surgery. It was concluded that the Android application was an accurate, efficient, and timely method for planning surgical variables.
 [DOI: 10.1117/1.JMI.4.1.015003]

Keywords: preoperative planning; Android application; brain shift; workflow; tumor; resection; neurosurgery; finite element; soft tissue; image-guided surgery; image guidance.

Paper 16270PR received Dec. 16, 2016; accepted for publication Feb. 13, 2017; published online Mar. 2, 2017.

1 Introduction

Image-guided neurosurgery (IGNS) relies on guidance systems that use preoperative images to provide visualization and facilitate surgical navigation within the brain.[1] In a recent review, Schulz et al.[2] considered 1400 papers over the previous 25 years and found 14 comparative studies for their analysis. The authors came to the conclusions that conventional IGNS reduces tumor burden, improves survival, reduces neurological deterioration, and does not have significant impact on the operating room (OR). They also went on to look at studies involving intraoperative magnetic resonance (iMR) imaging, which allows for soft-tissue image intraoperative updates as surgery progresses. The general finding was that accounting for soft tissue changes is desirable and that it improved survival times over conventional IGNS; however, the use of iMR systems has a considerable impact to the OR, surgical times, and expense.[2] Based on Schulz et al.'s review, image guidance and the compensation for soft tissue changes, also known as "brain shift," are highly desirable and cost-effective but accurate solutions would be of particular importance.

While methods using iMR,[3,4] intraoperative computed tomography (iCT),[5] and intraoperative ultrasound imaging[6,7] are being pursued for providing direct imaging data by conventional modalities to facilitate soft tissue changes, other approaches are in development. These approaches use data from intraoperative microscopes,[8,9] laser range scanners,[10,11] and conoscopic holography devices[12] in conjunction with advanced model-based image-to-physical registration approaches to compensate for deformations. Furthermore, while intraoperative imaging modalities, such as iMR and iCT, are quite compelling, workflow friendly, and inexpensive solutions using sparse data are certainly attractive; and there have been a variety of approaches[11,13–15] in this direction. We should note that while conventional IGNS essentially only requires that preoperative images be available to the neurosurgeon, these more advanced sparse-data-driven image-to-physical approaches can require significantly more preoperative processing. For example, in Ref. 16, the framework described requires (1) patient brain segmentation as well as subsurface structures, such as dural septa and tumors, (2) preoperative planning data acquisition, and (3) precomputations based on planning data. Other approaches are similar in needing preoperative segmentation and mesh building as well, e.g., Refs. 11 and 15. These types of processes do create more burdens, but if possible to realize in a workflow friendly manner, it does afford the ability to begin to explore other model-based enhancements to surgical procedures, which could have a dramatic impact in the OR theaters of the future.[17–19] However, this must be tempered with the reality that there are likely concurrent advances associated with preprocedural computations, which are needed for such advances to take place (e.g., robust segmentation, precomputational strategies, and sophisticated planners that are amenable to workflow).

*Address all correspondence to: Michael I. Miga, E-mail: Michael.I.Miga@vanderbilt.edu

2329-4302/2017/$25.00

In previous work, we have provided extensive algorithm development and testing of our sparse-data-driven model-based approach to brain shift correction in phantom, animal, and human studies (e.g., Refs. 14 and 20–23). However, we have not investigated the fidelity of preoperative planning steps, which are essential for the methodology and future prospective testing. In this work, we make a first contribution toward demonstrating the fidelity of our preoperative planning approach in a multisurgeon, multicase study. More specifically, using the framework associated with Ref. 16 as an exemplar, a set of surgical variables for tumor resection procedures are determined. In particular, three such variables are: (1) the expected head orientation for the procedure, (2) the expected craniotomy size and location, and (3) the expected trajectory to be taken into the tumor. These variables are essential for determining boundary conditions for our sparse-data-driven model-based nonrigid image-to-physical registration methodology. On a related note, having high confidence in the accuracy of the preoperatively planned variables would have a positive impact on the extent of preoperative computing time.[20] Similarly, a poorly designed planner could also negatively impact available surgeon time by being too slow and cumbersome, and consequently inhibit adoption. For example, in Ref. 16, the brain shift correction pipeline used a web-based desktop application to allow the neurosurgeon to manipulate three-dimensional (3-D) models of the patient's neuroanatomy and plan the surgical variables for the procedure. However, the application interface was not intuitive and proved to be incompatible with the day-to-day workflow of a practicing neurosurgeon, so much so that it could not be used routinely.

As a result, to improve the efficiency, simplicity, and accuracy of surgical variable acquisition, an Android, Java-based application was developed for tablet devices. Like its web-based predecessor as described above, the planner allows the neurosurgeon to manipulate 3-D models of the patient's head, brain, and tumor. These models are generated from the patient's preoperative segmented image volume using the Visualization Toolkit[24] and imported into our application called "Surgical Planner." The neurosurgeon uses the easy graphical touch interface of Surgical Planner to plan an expected head orientation, size and location of the craniotomy, and trajectory to be taken into the tumor. Once complete, these variables are exported through an e-mail client to the brain shift correction pipeline, where they are used in a series of preoperative computing tasks. Preliminary analysis regarding the development of Surgical Planner had been reported in Ref. 25. The proof-of-concept experiments performed in Ref. 25 involved a comparison study between the variables that a neurosurgeon generated using Surgical Planner for a particular case and the variables that the same neurosurgeon generated using a phantom head surgical setup for the same case. From that work, it was found that Surgical Planner was a good predictor of patient head orientation with respect to gravity and a good predictor of craniotomy size and centroid location. However, it was also found that further improvements in the application interface and phantom head surgical setup were needed and more surgical testing subjects were needed to improve performance. In the results reported herein, the Surgical Planner has been realized with the needed capabilities and more comprehensively tested with a mock operative setup and with multiple surgeons as well as multiple mock presentations. Finally, we should note that another fundamental contribution to the work is in the context of training. While some work has been achieved in this area[26] comparing virtual reality craniotomy planners to their traditional guidance counterpart, the metrics of performance were not quantitative and other surgical variables, such as overlap, precise centroid location, and accuracy of head orientation, were not assessed nor were these done in a multicase, multisurgeon comparison study.

2 Methods

2.1 *Development of Android Application*

Surgical Planner was designed using the Android platform and was written using Java and associated Java libraries. The OpenGL-ES-3.0 API was used to render 3-D graphics. A parser was developed that reads Legacy-ASCII .vtk files, which is a standard output file type for Visualization Toolkit 3-D models. Image-slice data were compiled using ITK-SNAP. 3-D CAD software (Sketchup) was used to design a virtual OR. The virtual OR was designed to loosely mimic a true surgical OR, in order to provide the surgeon with an intuitive visualization of the patient's neuroanatomy relative to the surgical environment. A Google Pixel C tablet was used during the development of the application, with 3 GB RAM and a Nvidia Tegra XI 64-bit processor.

Surgical Planner was designed to import patient data, provide an intuitive interface for head orientation, provide an intuitive interface for determining craniotomy location and area, provide an intuitive interface for determining trajectory, and export the planned surgical variables. Figures 1–3 show the Surgical Planner interface with accompanying descriptions below.

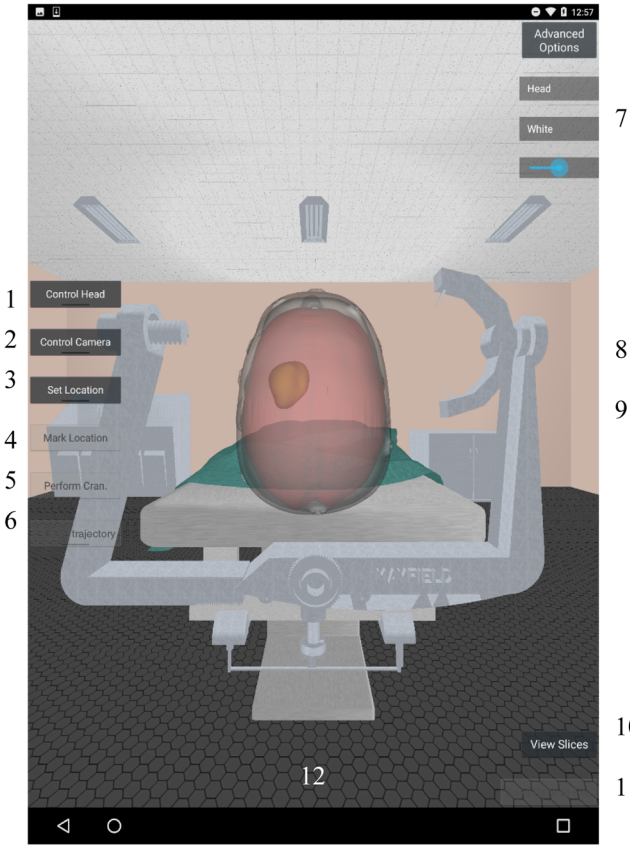

Fig. 1 Main Surgical Planner interface for head orientation planning.

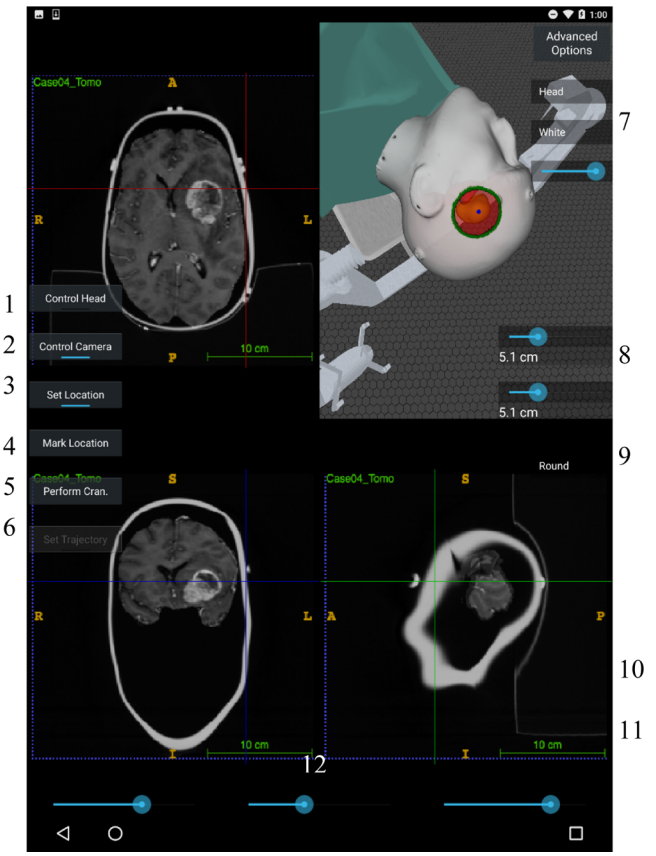

Fig. 2 Craniotomy planning mode in Surgical Planner.

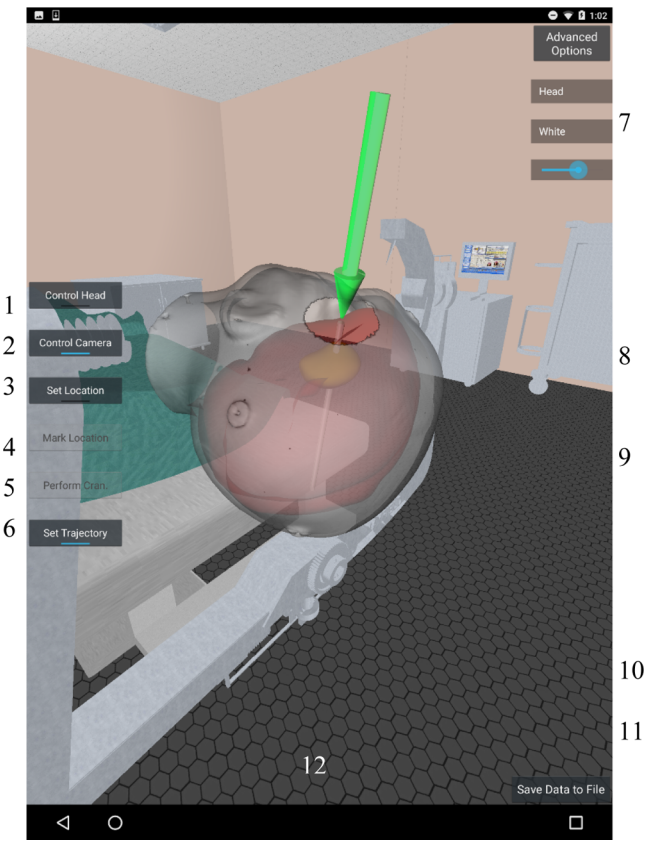

Fig. 3 Trajectory planning in Surgical Planner.

1. Control head

When selected, this allows the neurosurgeon to use touch gestures to freely rotate the patient's head. This feature can be used at any time during the planning process. This feature is typically used in conjunction with (10), in order to determine the head orientation for the tumor resection procedure. View slices/view models, described in more detail below, are features that allow the neurosurgeon to view the patient axial, coronal, and sagittal MR data (Figs. 1–3).

2. Control camera

This capability, when selected, allows the neurosurgeon to rotate the field of view around the operating table to view the patient's head from different angles. This feature can be used at any time during the planning process (Figs. 1–3).

3. Set location

This capability, when selected, allows the neurosurgeon to begin planning the craniotomy. Its activation switches the application into "craniotomy planning mode," and several user interface changes occur. The application interface splits into four distinct windows, as shown in Fig. 2. Three windows are used to display the patient's axial, coronal, and sagittal preoperative image slices. The last window shows a miniature display of the interface shown in Fig. 1. The activation of this feature, (3), results in the appearance of additional directional features [see slice data controls/craniotomy controls (12)] to move the craniotomy region around the patient's head. In addition, sliders for controlling the size of the craniotomy also appear [see adjust craniotomy shape (9)]. A dropdown box is also available for changing the craniotomy shape to either circular or rectangular [see (10)]. As the craniotomy region is translated around the patient's head, the center of the region is marked with crosshairs on the axial, coronal, and sagittal slice data (Fig. 2).

4. Mark location

As the craniotomy region is being determined using the features associated with (3), (4) will result in the appearance of a small green point at the center of the region. This serves as a method for marking important features on the surface of the head (such as the boundaries of the tumor relative to the surface of the head) (Fig. 2).

5. Perform craniotomy

This capability when activated finalizes the craniotomy region plan. If the neurosurgeon is unsatisfied with any of the parameters of this region after finalization (size, shape, and location), he or she can use (4), (9), (10), and (12) to plan the craniotomy region again, and perform craniotomy (5) to finalize the new plan (Fig. 2).

6. Set trajectory

This feature, when selected, allows the neurosurgeon to use touch gestures to rotate an arrow positioned at the center of the craniotomy region. The trajectory of this

arrow is extended into the patient's brain and tumor, so that the neurosurgeon can visualize the intersection of the trajectory with the tumor (Fig. 3).

7. Miscellaneous controls

   Somewhat less critical, there are additional capabilities in this area of the Surgical Planner interface that allow the neurosurgeon to make adjustments to the color and opacity of the patient's neuroanatomy (Figs. 1–3).

8. Adjust craniotomy size

   When (4) is selected, sliders will appear in region (8). These sliders allow the neurosurgeon to adjust the size of the craniotomy. The smallest possible craniotomy is 2.0 cm in total length, and the largest possible craniotomy is 12.0 cm in total length. For the cases studied, this range was found to be sufficient to express the surgeon's mock plan (Fig. 2).

9. Adjust craniotomy shape

   When (4) is selected, a dropdown box will appear in region (9). This dropdown box allows the neurosurgeon to choose between a circular or rectangular craniotomy region. The dimensions of this region are determined using (8) (Fig. 2).

10. View slices/view models

    When view slices are pressed, the app interface shows the patient's axial, coronal, and sagittal preoperative image slices. The neurosurgeon can use (12) to navigate through the slices and inspect the image volume. This feature is only used when planning the head orientation. After (3) is selected, the app interface changes to include the slice data [as described in (3)]. When view models are selected, the interface returns to the main app interface in Fig. 1.

11. Save data to file

    This capability, when activated, allows the neurosurgeon to export the data through an e-mail client on the tablet. The exported data contain a vector describing the direction of gravity in the rotated head relative to the original head position. This vector is determined by creating a rotation matrix that is dynamically updated based on touch gestures used to rotate the patient head and then applying this matrix to the original gravity unit vector. The data also contain a point cloud containing the Cartesian coordinates of the craniotomy region, and a vector that describes the trajectory to be taken into the tumor (determined using a similar process as the head orientation) (Fig. 3).

    The data are exported as both a .txt file and a .vtk file.

12. Slice data controls/craniotomy controls

    If (10) is selected, three sliders will appear in region (12). These sliders allow the neurosurgeon to navigate through the patient's axial, coronal, and sagittal slice image volume. If (3) is selected, a set of buttons will appear in region (12). These will allow the neurosurgeon to translate and rotate the craniotomy region around the head (Figs. 1 and 2).

2.2 *Assessing the Accuracy of Surgical Planner*

To assess the accuracy of the Surgical Planner, we began with a CT image volume of a phantom mannequin head. The CT image volume was then modified using a series of five patient MR image volumes containing tumors of various sizes, shapes, and locations from retrospective data as part of a Vanderbilt Institutional Review Board (IRB) approved study. Written patient consent was received for the use of all patient data utilized for this study and was approved by the Vanderbilt IRB. The set of five images contained tumors ranging from ~1.5 to 6 cm in diameter. Each MR image was properly scaled and fused with the CT image volume of the phantom head. Figure 4 is one example case. Table 1 shows the age, sex, location, and size of each patient used in this study. Figure 7 shows an axial and sagittal image slice of each case.

These fused images were then downloaded to the tablet containing Surgical Planner. A neurosurgeon with 20 years of experience, a neurosurgeon with 5 years of experience, a sixth-year neurosurgery resident, and a fifth-year neurosurgery resident all separately created tumor resection plans for each of the five images using the tablet application. With respect to the data reported below, the results of the surgeons have been randomly assigned to neurosurgeons 1, 2, 3, and 4, i.e., the neurosurgeon index does not correlate with experience.

Once complete, each neurosurgeon/resident was asked to simulate the same surgical plan on the phantom head using standard image-guided surgery approaches. The phantom head was mounted to a flexible rod, and this rod was mounted to a cart. In addition, a plastic torso was mounted to the cart, and the flexible rod was passed through the torso. Both the head and torso mounts are capable of vertical movement, allowing the neurosurgeon to effectively adjust the height of the "patient bed" relative to the ground. The flexible rod allows the neurosurgeon to freely position the head, and the presence of the torso allows the neurosurgeon to determine if a particular head configuration is physically realistic (Fig. 5).

For a particular case, the neurosurgeon was asked to view the case's fused image data through 3-D Slicer[27] in order to establish a geometric understanding of tumor size and location. Using this knowledge, the neurosurgeon chose a suitable orientation for the phantom head. Image-to-physical space registration was then performed using the Fiducial Registration Wizard (SlicerIGT extension), OpenIGTLinkIF, and the PLUS toolkit,[28] an application that streams live tracking data to 3-D Slicer. The point-based registration was performed by selecting the center points of MR-CT-visible markers attached to the phantom head. Physical space fiducial centers were digitized in 3-D Slicer using OpenIGTLinkIF and the PLUS toolkit (Fig. 6). All physical space measurements were performed using a Northern Digital Polaris Spectra (NDI, Waterloo, Ontario, Canada). Following registration, the neurosurgeon used the image guidance system and a stylus to mark the craniotomy and tumor boundaries and draw the craniotomy contour on the surface of the head with a marker. A custom OpenIGT extension that collects points in physical space and converts them to image space was used to collect the points on the surface of the head corresponding to the craniotomy contour, relative to image space. In addition, the orientation of the head was determined by collecting three coplanar points on a flat, horizontal surface. The cross product of two vectors created from these points gave the direction that gravity is acting on the head, relative to image space. Finally, the neurosurgeon was asked to hold a metal rod

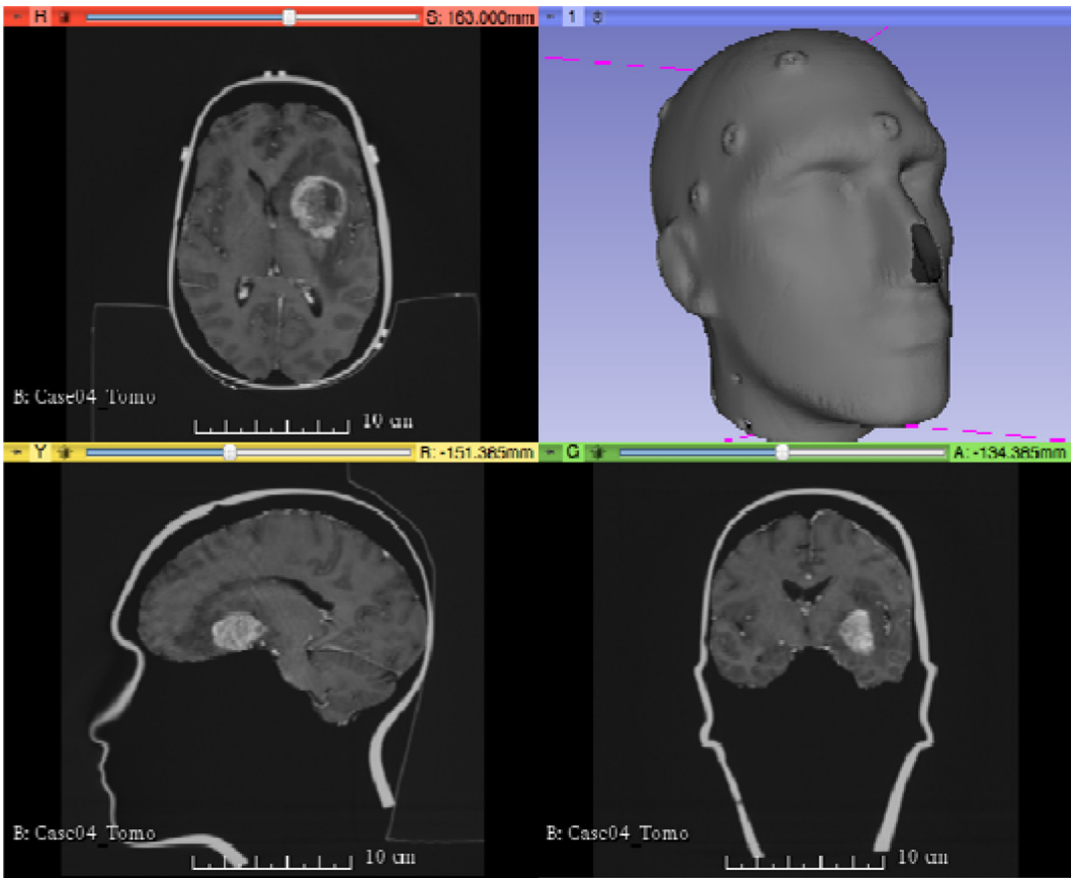

Fig. 4 Example of fused images viewed on 3-D Slicer.

in the intended trajectory to be taken into the tumor, and two points were collected, corresponding to each end of the rod, in order to create a vector representing trajectory in image space.

The angle difference between the Surgical Planner gravity vector and the physical gravity vector for each case was determined. The surface area and centroid difference between the Surgical Planner craniotomy region and physical craniotomy region for each case were also determined. A Sørensen–Dice (DICE) coefficient was also calculated to determine the degree of overlap between both regions.[29] The DICE coefficient is a statistic that compares the degree of overlap between two sets of data, with DICE = 1 indicating a perfect overlap of data points.

Table 1 Patient information and tumor details.

Case	Age	Sex	Tumor location	Tumor size (cm^3)
A	37	F	LF	1.2
B	64	M	MF	12.6
C	57	F	RF	5.1
D	52	F	RF	2.4
E	51	F	LT	31.8

Note: Tumor location is specified using the following abbreviation nomenclature: L, left; R, right; M, medial; T, temporal; F, frontal; and P, parietal.

3 Results

Summaries of the results of the comparison study are shown in Tables 2–6. Figure 7 illustrates the mock patient MR data that were used to plan physical craniotomies. Figure 8 illustrates an example result of tablet-plan-to-physical-plan craniotomy with

Fig. 5 Physical setup (head and torso mounted to cart).

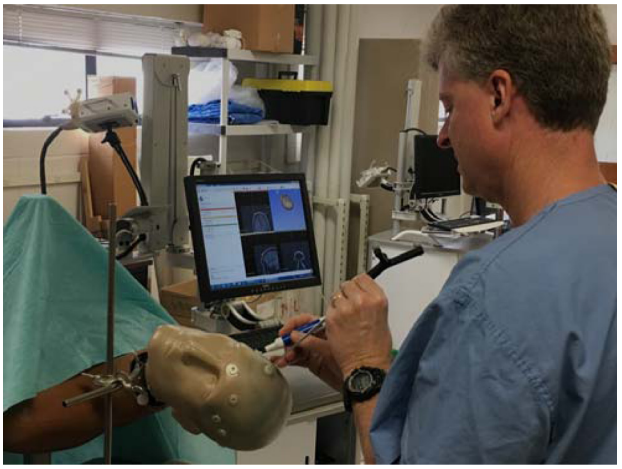

Fig. 6 Neurosurgeon planning craniotomy boundary.

respect to localization and area overlap for each of the mock cases.

Table 2 shows the head orientation angle differences between the Surgical Planner plan and the physical plans. On average, there was 14.1 ± 6.8 deg of difference between both plans for all surgeons and all cases. Case A was found to have the least angle difference, on average, across all surgeons, while case C was found to have the greatest angle difference. These angle difference values are marked in bold and italic, respectively, in Table 2 in the last column. Neurosurgeons 1 and 4 had the lowest and highest angle differences, respectively. These angle difference values are marked in bold and italic, respectively, in Table 2, columns 2 and 5, respectively.

In addition, a Kruskal–Wallis test was performed on the data in Table 2 to assess if there were differences in head orientation differences between neurosurgeons, and it was found that there was no significant difference between neurosurgeons ($p = 0.6443$ and $\alpha = 0.05$). Similarly, a Kruskal–Wallis test was performed on the data in Table 2 to assess if there were differences in head orientation differences between cases, and it was found that there was no significant difference between cases ($p = 0.6746$ and $\alpha = 0.05$).

Table 3 shows the craniotomy centroid differences between the Surgical Planner plan and the physical plan for each respective trial. On average, the craniotomy centroid difference was 7.1 ± 3.4 mm. Case A had the smallest centroid difference, on average, across all surgeons, while case B had the largest centroid difference. Neurosurgeon 2 had the smallest centroid difference, on average, across all cases, whereas neurosurgeon 1 had the greatest centroid difference.

Neurosurgeon 1 had a large craniotomy centroid difference of 24 mm for case C and neurosurgeon 3 had a large craniotomy centroid difference of 37 mm for case D. These two cases were neglected in the calculations of the average centroid differences due to experimental system design failures. With each, the experimental system failed for different reasons and these are described in Sec. 4. With respect to how these experiments are conducted, head positioning is the first phase of the experiment, while interaction for craniotomy plan is a second phase; as

Table 2 Head orientation angle difference between Surgical Planner and physical plan.

Unit: deg	Neurosurgeon 1	Neurosurgeon 2	Neurosurgeon 3	Neurosurgeon 4	Average: cases
Case A	2.9	5.8	8.2	26.5	**10.9 ± 10.6**
Case B	6.8	19.3	9.7	14.7	12.6 ± 5.5
Case C	15.7	14.2	23.2	19.3	*18.1 ± 4.0*
Case D	5.9	20.1	17.2	16.5	14.9 ± 6.2
Case E	20.7	10.3	19.8	4.8	13.9 ± 7.7
Average: surgeons	**10.4 ± 7.5**	13.9 ± 6.0	15.6 ± 6.5	*16.4 ± 7.9*	14.1 ± 6.8

Note: Bold and italicized results represent best and worst results, respectively, in respective comparison.

Table 3 Craniotomy centroid difference between Surgical Planner and physical plan.

Unit: mm	Neurosurgeon 1	Neurosurgeon 2	Neurosurgeon 3	Neurosurgeon 4	Average: cases
Case A	9.3	1.0	4.5	3.7	**4.6 ± 3.5**
Case B	7.2	6.1	10.3	12.3	*9.0 ± 2.9*
Case C	—	8.3	3.2	12.1	7.9 ± 4.5
Case D	11.2	5.8	—	9.9	9.0 ± 2.8
Case E	7.4	5.1	4.2	2.9	4.9 ± 1.9
Average: surgeons	*8.8 ± 1.8*	**5.3 ± 2.7**	5.6 ± 3.2	8.2 ± 4.6	7.1 ± 3.4

Note: Bold and italicized results represent best and worst results, respectively, in respective comparison.

Table 4 Craniotomy surface area difference (physical plan area–Surgical Planner area).

Unit: mm^2	Neurosurgeon 1	Neurosurgeon 2	Neurosurgeon 3	Neurosurgeon 4	Average: cases
Case A	132	−370	749	41	**138 ± 462**
Case B	394	685	858	1040	*744 ± 275*
Case C	—	−17	284	754	340 ± 389
Case D	147	721	—	469	446 ± 288
Case E	494	−187	839	581	432 ± 438
Average: surgeons	292 ± 181	**166 ± 506**	*683 ± 270*	577 ± 369	429 ± 396

Note: Bold and italicized results represent best and worst results, respectively, in respective comparison.

Table 5 Craniotomy overlap between Surgical Planner and physical plan, using DICE coefficient.

Unitless	Neurosurgeon 1	Neurosurgeon 2	Neurosurgeon 3	Neurosurgeon 4	Average: cases
Case A	0.92	0.89	0.76	0.95	**0.88 ± 0.08**
Case B	0.62	0.74	0.81	0.49	*0.67 ± 0.14*
Case C	—	0.66	0.87	0.59	0.71 ± 0.15
Case D	0.79	0.71	—	0.86	0.79 ± 0.08
Case E	0.74	0.78	0.71	0.72	0.74 ± 0.03
Average: surgeons	0.77 ± 0.12	0.76 ± 0.09	**0.79 ± 0.07**	*0.72 ± 0.19*	0.76 ± 0.12

Note: Bold and italicized results represent best and worst results, respectively, in respective comparison.

Table 6 Elapsed time using Surgical Planner.

Unit: min:s	Neurosurgeon 1	Neurosurgeon 2	Neurosurgeon 3	Neurosurgeon 4	Average: cases
Case A	04:57	04:35	04:56	02:56	04:21 ± 00:58
Case B	04:07	04:58	06:50	02:19	*04:34 ± 01:53*
Case C	06:04	04:47	05:19	01:48	04:30 ± 01:52
Case D	04:43	03:58	06:32	02:27	04:25 ± 01:42
Case E	04:21	04:45	05:35	02:15	**04:14 ± 01:25**
Average: surgeons	04:50 ± 00:45	04:37 ± 00:23	*05:50 ± 00:49*	**02:21 ± 00:24**	04:25 ± 01:26

Note: Bold and italicized results represent best and worst results, respectively, in respective comparison.

such, head positioning was considered unaffected in Table 2 and all values are reported.

In addition, a Kruskal–Wallis test was performed on the data in Table 3 to assess if there were differences in craniotomy centroid differences between neurosurgeons, and it was found that there was no significant difference between neurosurgeons ($p = 0.3702$ and $\alpha = 0.05$). Similarly, a Kruskal–Wallis test was performed on the data in Table 3 to assess if there were differences in craniotomy centroid differences between cases, and it was found that there was no significant difference between cases ($p = 0.1904$ and $\alpha = 0.05$).

Table 4 shows the craniotomy surface area differences between the Surgical Planner plans and the physical plans. The surface area difference was calculated by subtracting the Surgical Planner craniotomy surface area from the physical craniotomy surface area. The average surface area difference was 429 ± 396 mm^2. Case A had the smallest surface area difference, on average, across all surgeons, while case B had the largest surface area difference. Neurosurgeon 2 had the smallest surface area difference across all cases, whereas neurosurgeon 3 had the largest surface area difference. As referenced earlier, Neurosurgeons 1 and 3 experienced a system failure in two instances of the experiment. Given that the data associated with Table 4 are associated with the same phase of the experiment as that of Table 3, it was neglected in the averages.

In addition, a Kruskal–Wallis test was performed on the data in Table 4 to assess if there were differences in surface area differences between neurosurgeons, and it was found that

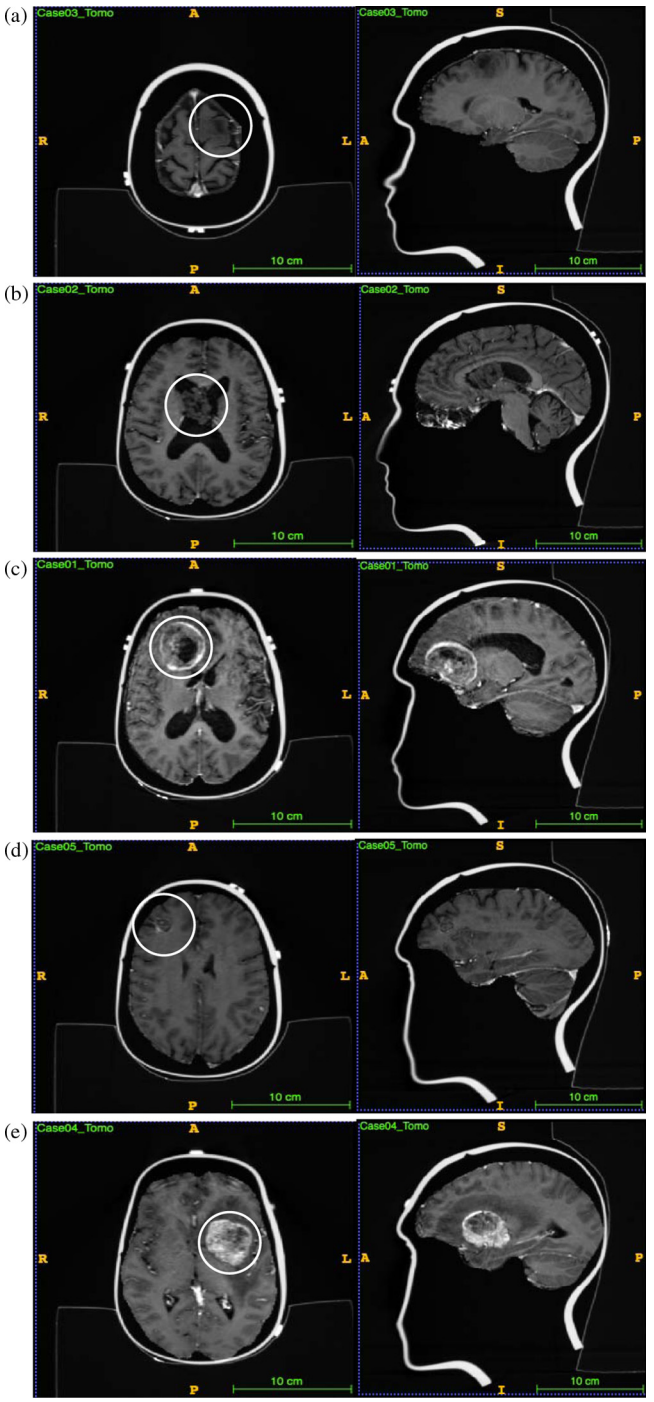

Fig. 7 Axial and sagittal image slices of the tumor for each mock case. White circle shows lesion.

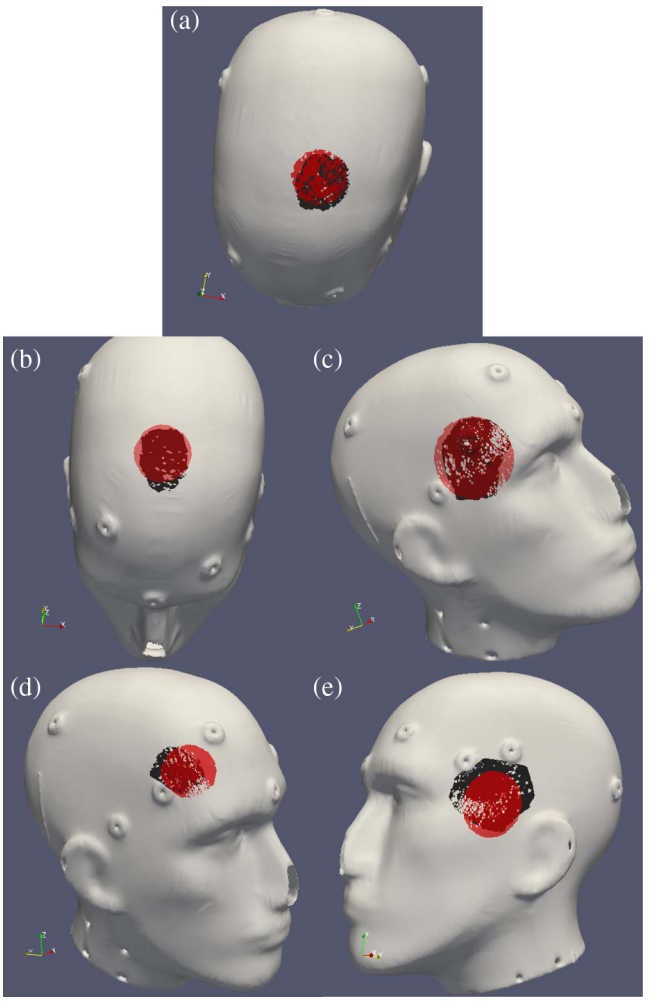

Fig. 8 Surgical Planner craniotomy (red) overlays on physical craniotomy (black). Each image represents the best craniotomy result for that particular case.

there was no significant difference between neurosurgeons ($p = 0.1386$ and $\alpha = 0.05$). Similarly, a Kruskal–Wallis test was performed on the data in Table 4 to assess if there were differences in surface area differences between cases, and it was found that there was no significant difference between cases ($p = 0.3534$ and $\alpha = 0.05$).

Table 5 shows the craniotomy overlap between the Surgical Planner craniotomy regions and the physical craniotomy regions, expressed using a DICE coefficient. The average DICE coefficient across all cases, across all surgeons, was 0.76 ± 0.12. Case A had the best overall craniotomy overlap across all surgeons, whereas case B had the worst overall craniotomy overlap. Neurosurgeon 3 had the best overall craniotomy overlap across all cases, whereas neurosurgeon 4 had the worst craniotomy overlap across all cases. As referenced earlier, two experimental instances associated with neurosurgeons 1 and 3 were neglected due to system failure. Given that the data associated with Table 5 are acquired during this same craniotomy planning phase as Tables 3 and 4, these instances were neglected in the calculation of the DICE coefficient averages.

In addition, a Kruskal–Wallis test was performed on the data in Table 5 to assess if there were differences in DICE coefficients between neurosurgeons, and it was found that there was no significant difference between neurosurgeons ($p = 0.9016$ and $\alpha = 0.05$). Similarly, a Kruskal–Wallis test was performed on the data in Table 5 to assess if there were differences in DICE coefficients between cases, and it was found that there was no significant difference between cases ($p = 0.1305$ and $\alpha = 0.05$).

Table 6 shows the average amount of time, in min:s, that was taken to complete each case on Surgical Planner. On average, it took $04:25 \pm 01:26$ min :s to plan a case on Surgical Planner. It took the least amount of time to plan case E across all surgeons, and it took the most time to plan case B. Neurosurgeon

3 took the longest time to plan all the cases on average using the Surgical Planner, whereas neurosurgeon 4 took the least time on average.

While Tables 2–6 provide a great deal of quantitative data regarding the performance of Surgical Planner with respect to head orientation, craniotomy planning, and time used, they do not provide a sense of performance. Figures 8(a)–8(e) illustrate the best craniotomy overlap placements across the five different cases. As a reference, Fig. 8(e) represents a result that is quite close to the average DICE result (~2% of average). Last, Fig. 8 also illustrates quite nicely the varied position of tumors for assessing the testing approach undertaken in this work.

4 Discussion

Table 7 provides summaries of the results. The brain shift computational pipeline associated with Ref. 20 creates a 20-deg conical capture range of possible head orientations from the user-prescribed predicted head orientation in order to account for variability between the preoperatively planned head orientation and actual OR head orientation. As indicated in Ref. 20, when true head orientations begin to deviate by more than 5 deg outside the capture range, the performance of our nonrigid image-to-physical registration method tended to suffer. As a result, it is important that that the head orientation angle difference between Surgical Planner and the physical plan consistently falls within this range. As can be seen in Table 7, the average deviation is well within our typical 20 deg working conical range. To further support this observation, a Wilcoxon rank-sum test was performed on the data in Table 1 and it was found that the global mean ($\mu = 14.1$ deg) was significantly <20 deg (H0: $\mu = 20$ deg, H1: $\mu > 20$ deg, $p = 0.9988$). However, 4 of the 20 attempts fell outside the 20-deg capture range with a maximum deviation of 26.5 deg. As a result, extending that conical capture range to ± 30 deg will be considered in the future. Nevertheless, the results of the comparison study prove that Surgical Planner can predict the OR head orientation with very good accuracy.

With regards to craniotomy planning, in the cases of brain "sag" due to the reduction in buoyancy forces, the relevance of accurate craniotomy size with respect to our model-based image-to-physical nonrigid registration approach is not relevant since the strategy for applying boundary conditions in this region is not affected. However, in the cases of brain swelling, craniotomy size may play an important role. As Table 7 reports, the average discrepancy is on the order of a 2-cm^2 collective area patch. While at this time further investigation of our correction pipeline is needed to determine the effect of this variability, we would suggest that the impact is likely minimal. More specifically, brain swelling is often mitigated prior to disruption of the brain surface. This is not to say that swelling is not useful in a compensation approach; but rather, thankfully in our work, the incorporation of swelling conditions for use in correction has been found to be quite limited (e.g., in Ref. 13, swelling solutions only influenced about 10% of reconstructed deformations). Nevertheless, the results in Table 7 are promising.

Table 7 Comparison metrics and corresponding average values.

Comparison metric	Average value
Head orientation	14.1 ± 6.8 deg
Centroid difference	7.1 ± 3.4 mm
Surface area difference	429 ± 396 mm^2
DICE coefficient	0.76 ± 0.12
App planning time	$04{:}25 \pm 01{:}26$ (min:s)

With respect to craniotomy centroid and overlap comparisons between Surgical Planner and physical plan, we see a 7.1-mm difference and an average DICE coefficient of 0.76. This indicates that Surgical Planner is a very good predictor of the centroid and overlap. For our exemplar in Ref. 16, the visible cortical surface is an important source of data to drive the pipeline. For example, image-to-physical registration strategies have exploited the Gadolinium-enhanced MR images for direct cortical surface registration or use within resection approaches as in Refs. 20 and 30 or in the area of cortical surface vessel tracking as in Ref. 9.

Going further with respect to craniotomy metrics, specifically centroid and surface area, as we look at the results of Fig. 8 in light of Tables 3 and 4, it is interesting to note the consistency of localizing the centroid between virtual and physical plans where the standard deviation of the difference is less than half of the associated error. Whereas with the craniotomy surface extent error, the standard deviation is on the same order as the difference magnitude itself between the virtual and physical plans. While somewhat anecdotal, we did observe a functional change between these functions when using the respective planners. Beginning with the physical plan, surgeons tended to use the optically tracked stylus to determine the centroid and then moved the stylus to tumor extents to begin to demark the borders of the craniotomy. While the former designation of the centroid was done very similar to the physical plan counterpart using the virtual planner (feature associated with Fig. 2), the latter designation of craniotomy surface extent was done quite differently. Briefly, despite a similar stylus-like capability being available with the virtual planner, the surgeons found this to be somewhat cumbersome and estimated the extent using a 3-D view of the tumor/head system from the main visualization view (Fig. 1). In some respects, this is a strategy that elects to discard imaging information in favor of ease. Again, while the alteration to the procedure was observational, detailed impact is not available. However, we do see that in 15 of 18 plans (Table 4), the virtual planner underestimated the craniotomy extent that provides some quantitative data on the difference between physical and virtual plans.

The average DICE coefficient between the Surgical Planner craniotomy regions and the physical craniotomy regions indicates that Surgical Planner is a good predictor of the physical craniotomy region. The discrepancies could be explained principally by the surface area differences and shape differences between the Surgical Planner craniotomy regions and the physical plan counterparts. In Fig. 8, the differences between the Surgical Planner's systematic geometric craniotomy shapes and the physical plan counterparts can easily be discerned.

With respect to time expended, it took surgeons an average of 4 min and 25 s to plan a case on Surgical Planner, with a range of 1 min and 48 s to 6 min and 50 s. These results support the notion that Surgical Planner is a quick and efficient method for obtaining surgical variables for a brain-tumor resection procedure. We should also note that while each physician was trained on Surgical Planner and did plan multiple virtual

Table 8 Ranking of surgeon performance for each comparison metric.

	Ranked first	Ranked fourth
Head orientation	Neurosurgeon 1	Neurosurgeon 4
Centroid difference	Neurosurgeon 2	Neurosurgeon 1
Surface area difference	Neurosurgeon 2	Neurosurgeon 3
DICE	Neurosurgeon 3	Neurosurgeon 4
Time	Neurosurgeon 4	Neurosurgeon 3

surgeries, overall, this still represented a limited experiential setting. It would be interesting to extend these studies and see if performance and speed would improve.

While attempting to correlate differences in planning accuracy versus neurosurgeon experience level was not examined and is not appropriate due to limited sampling (i.e., $n = 1$ surgeon from each experience level), it is interesting to look across Tables 2–6 at the best performances in each respective metric. It is interesting to note that all of the surgeons who participated ranked first in at least one metric, and each except one ranked fourth in at least one metric. Neurosurgeon 2 was the only subject who did not rank fourth in a metric. While these results are interesting, it does lead one to speculate as to whether there is an added direction in this work akin to the fundamentals of laparoscopic surgery testing. Could such a tool be used as an in a silico/phantom environment for training neurosurgeons for image-guided surgery procedures? (Table 8)

In addition to performance, differences in the planning accuracy among cases were also examined (Table 9). It was found that cases A and E had the best results overall, whereas cases B and D had the worst results overall. A possible explanation for this result is that case D consisted of a small, tumor with poor contrast (<2 cm in diameter) that was more challenging to see in the image volume (Fig. 7). Also, with regards to case B, it was discovered that the tumor was not properly segmented from the image volume. The segmentation was an underestimate of the true extent of the tumor. As a result, the 3-D tumor that was uploaded in the app was not a fully accurate representation of the true extent of the tumor in the image volume. This may explain the large and systematic underestimation of the physical craniotomy region size by the Surgical Planner regions for case B, as shown in Table 4. This may also explain the large craniotomy differences and low DICE coefficients that were observed for this case. Case E was a large tumor that was clearly visible in the image volume, and case A, despite not being a particularly large tumor, was located close to the surface of the brain and was easily locatable. A potential source of error in the physical experiment was the manual contrast level adjustments that were made prior to the mock physical procedure for each case. It was difficult to consistently apply the same contrast adjustments for multiple trials of a particular case with multiple surgeons (more discussion below on this concerning case D for neurosurgeon 3).

With respect to the studies conducted in this work, there were several limitations that are primarily associated with the experimental procedure and physical apparatus used in the study. The ideal workflow for Surgical Planner involves the neurosurgeon downloading a patient's case data from a private e-mail server, generating a set of surgical variables for that data, and exporting these variables back to the preoperative computing framework via private e-mail. This would typically be done at least a day in advance of surgery.[16] On the day of surgery, the surgeon would perform surgery while the brain shift correction pipeline updated the guidance system. While every attempt was made to mimic this workflow, it was difficult to have neurosurgeons perform a plan on the Surgical Planner on one day and then perform the physical procedure on the following day, due to scheduling conflicts. Thus, data were sometimes collected with a week-long interval between sessions, which could have influenced accuracy.

Another limitation concerned the use of a mannequin head on a flexible mount that allowed the neurosurgeon to move the mannequin head freely. Surgical Planner also allows the neurosurgeon to rotate the patient's head freely. However, an actual human patient has a limited range of head orientations that can be performed due to the presence of the neck. To address this, the physical apparatus in this experiment used a torso to restrict the mobility of the mannequin head and allows the neurosurgeon to visually assess the realism of a given head orientation. However, no such restriction was given in Surgical Planner. The absence of human head features, such as the eyebrows and hairline, as well as the geometry of the human head also contributed to the nonideality of the physical setup.

Last, as mentioned in both Secs. 3 and 4, neurosurgeons 1 and 3 performed one plan each that had large craniotomy centroid differences, large surface area differences, and low DICE coefficients. Those cases were indicated with "—" symbols in Tables 3–5. For neurosurgeon 1, there was an inability to accurately locate the tumor on the guidance system due to the nonideal nature of the mannequin head. The head did not have traditional features that are present in a normal human head

Table 9 Ranking of cases by overall surgeon accuracy for each comparison metric.

	Rank 1	Rank 2	Rank 3	Rank 4	Rank 5
Head orientation	Case A	Case B	Case E	Case D	Case C
Centroid difference	Case A	Case E	Case C	Case D	Case B
Surface area difference	Case E	Case A	Case C	Case D	Case B
DICE	Case A	Case D	Case E	Case C	Case B
Time	Case E	Case A	Case D	Case C	Case B

(eyebrows and hairline), and as a result, neurosurgeon 1 had difficulty with intuitively localizing the tumor in the mannequin head. Ultimately, the artificial nature of the head did not provide neurosurgeon 1 with the routine features that would normally be used to plan a craniotomy for that particular tumor location.

Unlike the error for neurosurgeon 1, for neurosurgeon 3, the error in the planned case was due to poor image contrast in the image volume that affected the neurosurgeon's ability to accurately locate the tumor on the guidance system. It was determined retrospectively that the app-predicted craniotomy was a close estimate to the ideal craniotomy for resecting this tumor, and the physical craniotomy did not resemble the more conventional craniotomy because of the poor contrast level used to display the image volume in the guidance system. Both of these errors by neurosurgeons 1 and 3 ultimately reflected errors in the physical plan tumor-identification procedure. Thus, these two cases were neglected when calculating the averages in Tables 3–5. We should also note that when testing across all data in Table 1, the Shapiro–Wilk normality test was positive at $p = 0.01$ indicating the data were normal. Similarly, analyzing the data in Tables 3–5 without the functional failures also tested positive for normality at $p = 0.01$. While observational, this would seem to suggest that excluding these system failures did not change the quality of the experiment as normality was maintained.

5 Conclusions

Overall, it was determined that development of a tablet-based application for rapid preplanning of surgeries, such as Surgical Planner, is a viable direction for acquiring preoperatively accurate estimates of OR surgical variables for brain-tumor resection procedures. In this particular realization, the Surgical Planner allowed surgeons to predict head orientation, craniotomy centroid location, and craniotomy shape with very good accuracy. In addition, the surface area of the craniotomy region designated by Surgical Planner was representative of the actual OR craniotomy region surface area. Also, the results of this study indicate that the Surgical Planner is a timely and efficient method for determining surgical variables for brain-tumor resection procedures. The intuitive virtual interface allows neurosurgeons to quickly obtain and upload data files for a case on Surgical Planner and quickly export the planned surgical variables for that case through an e-mail/network client.

Given the overall positive performance of Surgical Planner in predicting surgical variables, it is interesting to speculate on the role of such user-friendly applications for tablet and phone computing. To our knowledge, this is the first testing of such an application interface within the context of planning IGNS for the purpose of deformation correction strategies. When we consider a cost-conscious healthcare system, the demands on physician time are such that they preclude extensive preoperative planning. As a result, the use of more sophisticated computational platforms for the OR or interventional suite is likely to remain inhibited. However, the wealth of information and analysis that high fidelity computing could provide intraoperatively compels us to overcome this challenge. The work presented here is a first step in efficient precomputation-enabling mobile tablet platforms and the considerable promise of such tablet applications. With the realization of efficient preoperative planning tools that can be driven by the expertise of the surgeon and yet are fast and accurate and minimally disrupting of the surgeon's day-to-day workflow, this may represent a fundamental transformative pathway for the integration of computing platforms to drive intraoperative procedures.

Disclosures

No conflicts of interest (financial or otherwise) are declared by the authors.

Acknowledgments

This work was supported by the National Institute for Neurological Disorders and Stroke of the National Institutes of Health under Grant No. R01NS049251.

References

1. R. L. Galloway, "The process and development of image-guided procedures," *Annu. Rev. Biomed. Eng.* **3**, 83–108 (2001).
2. C. Schulz, S. Waldeck, and U. M. Mauer, "Intraoperative image guidance in neurosurgery: development, current indications, and future trends," *Radiol. Res. Pract.* **2012**, 197364 (2012).
3. A. Nabavi et al., "Serial intraoperative magnetic resonance imaging of brain shift," *Neurosurgery* **48**, 787–797 (2001).
4. C. Nimsky et al., "Quantification of, visualization of, and compensation for brain shift using intraoperative magnetic resonance imaging," *Neurosurgery* **47**, 1070–1080 (2000).
5. P. Gasinski et al., "Application of intraoperative computed tomography in a neurosurgical operating theatre," *Neurol. Neurochir. Pol.* **46**, 536–541 (2012).
6. G. Unsgaard et al., "Intra-operative 3D ultrasound in neurosurgery," *Acta Neurochir.* **148**, 235–253 (2006).
7. H. Rivaz, S. J.-S. Chen, and D. L. Collins, "Automatic deformable MR-ultrasound registration for image-guided neurosurgery," *IEEE Trans. Med. Imaging* **34**, 366–380 (2015).
8. H. Sun et al., "A noncontacting 3-D digitizer for use in image-guided neurosurgery," *Stereotactic Funct. Neurosurg.* **80**, 120–124 (2004).
9. S. Ding et al., "Tracking of vessels in intra-operative microscope video sequences for cortical displacement estimation," *IEEE Trans. Biomed. Eng.* **58**, 1985–1993 (2011).
10. M. I. Miga et al., "Cortical surface registration for image-guided neurosurgery using laser-range scanning," *IEEE Trans. Med. Imaging* **22**, 973–985 (2003).
11. D. X. Zhuang et al., "A sparse intraoperative data-driven biomechanical model to compensate for brain shift during neuronavigation," *Am. J. Neuroradiol.* **32**, 395–402 (2011).
12. A. L. Simpson et al., "Evaluation of conoscopic holography for estimating tumor resection cavities in model-based image-guided neurosurgery," *IEEE Trans. Biomed. Eng.* **61**, 1833–1843 (2014).
13. I. Chen et al., "Intraoperative brain shift compensation: accounting for dural septa," *IEEE Trans. Biomed. Eng.* **58**, 499–508 (2011).
14. P. Dumpuri et al., "An atlas-based method to compensate for brain shift: preliminary results," *Med. Image Anal.* **11**, 128–145 (2007).
15. S. Ji et al., "Data assimilation using a gradient descent method for estimation of intraoperative brain deformation," *Med. Image Anal.* **13**, 744–756 (2009).
16. K. Sun et al., "Near real-time computer assisted surgery for brain shift correction using biomechanical models," *IEEE J. Transl. Eng. Health Med.* **2** (2014).
17. C. R. Butson et al., "Patient-specific analysis of the volume of tissue activated during deep brain stimulation," *NeuroImage* **34**, 661–670 (2007).
18. E. Yeniaras et al., "Design and initial evaluation of a treatment planning software system for MRI-guided laser ablation in the brain," *Int. J. CARS* **9**, 659–667 (2014).
19. P. R. Jackson et al., "Patient-specific mathematical neuro-oncology: using a simple proliferation and invasion tumor model to inform clinical practice," *Bull. Math. Biol.* **77**, 846–856 (2015).
20. I. Chen et al., "Integrating retraction modeling into an atlas-based framework for brain shift prediction," *IEEE Trans. Biomed. Eng.* **60**, 3494–3504 (2013).

21. M. I. Miga et al., "In vivo quantification of a homogeneous brain deformation model for updating preoperative images during surgery," *IEEE Trans. Biomed. Eng.* **47**(2), 266–273 (2000).
22. M. I. Miga et al., "Model-updated image guidance: initial clinical experience with gravity-induced brain deformation," *IEEE Trans. Med. Imaging* **18**(10), 866–874 (1999).
23. M. I. Miga et al., "Clinical evaluation of a model-updated image-guidance approach to brain shift compensation: experience in 16 cases," *Int. J. CARS* **11**(8), 1467–1474 (2016).
24. W. Schroeder, K. Martin, and B. Lorensen, *The Visualization Toolkit: An Object-Oriented Approach to 3D Graphics*, Prentice Hall, New Jersey (1996).
25. R. C. Vijayan et al., "Determination of surgical variables for a brain shift correction pipeline using an android application," *Proc. SPIE* **9786**, 978610 (2016).
26. A. T. Stadie et al., "Neurosurgical craniotomy localization using a virtual reality planning system versus intraoperative image-guided navigation," *Int. J. CARS* **6**(5), 565–572 (2011).
27. A. Fedorov et al., "3D Slicer as an image computing platform for the quantitative imaging network," *Magn. Reson. Imaging* **30**, 1323–1341 (2012).
28. A. Fedorov et al., "3D slicer as an image computing platform for the quantitative imaging network," *Magn. Reson. Imaging* **30**, 1323–1341 (2012).
29. K. H. Zou et al., "Statistical validation of image segmentation quality based on a spatial overlap index," *Acad. Radiol.* **11**, 178–189 (2004).
30. A. Cao et al., "Laser range scanning for image-guided neurosurgery: investigation of image-to-physical space registrations," *Med. Phys.* **35**, 1593–1605 (2008).

Rohan C. Vijayan is a fourth year biomedical engineering undergraduate student at Vanderbilt University.

Rebekah H. Griesenauer is a PhD candidate of biomedical engineering at Vanderbilt University.

Michael I. Miga received his PhD in biomedical engineering from Dartmouth College in 1998. He joined Vanderbilt University in spring of 2001 and is the Harvie Branscomb professor at Vanderbilt. He is a professor of biomedical engineering, radiology, and neurological surgery. He is the Biomedical Modeling Laboratory director and cofounder of the Vanderbilt Institute in Surgery and Engineering. His research interests are in computational modeling and inverse problems for therapeutic applications and imaging.

Biographies for the other authors are not available.